Ionizing beam tracking in gaseous chambers for field mapping

T. Jalowy, R. Neugebauer, and K. O. Groeneveld
Institut für Kernphysik der J. W. Goethe Universität, August-Euler-Strasse 6, D-60486 Frankfurt am Main, Germany

C. R. Ponciano, L. S. Farenzena, and E. F. da Silveira[a)]
Departamento de Fisica, Pontifícia Universidade Católica, CP 38071, Rio de Janeiro 22452-970, Brazil

(Received 7 January 2002; accepted for publication 23 April 2002)

The combination of the time-of-flight (TOF) technique with two-dimensional position-sensitive (*XY*) ion detection is employed for tracking projectile-gas collisions. The main goal is to determine the detailed distribution of local electric fields, which accelerate the gas ions produced in the collisions. A low-pressure target gas spectrometer for this goal is described and all necessary *XY*-TOF expressions concerning the ion dynamics are presented. Experimental results of a 150 keV neutral H beam colliding with a He–Ne–Ar mixture are compared with the calculations. The new method can also be used for mapping magnetic fields or in large collision gas cells, e.g., to increase resolution in mass spectrometry and to perform initial momentum measurements of the produced ions. © *2002 American Institute of Physics.* [DOI: 10.1063/1.1498909]

I. INTRODUCTION

Time-of-flight (TOF) analysis of ions produced in gaseous target fast particle impact has been performed for a long time.[1–5] One of the main improvements on this subject was carried out by Wiley and McLaren[3] in 1955, with the introduction of pulsed ion extraction in a two-stage spectrometer. This time-focusing principle has been used since in many TOF spectrometer types and for different ionizing beams: photons (pulsed laser or synchrotron light), electrons, fast atoms, or ions.[1]

In order to improve mass resolution, sensitivity, or dynamical range of gas spectrometers, new techniques have been added: pulsed extraction fields,[6] tandem setup[1] (MS–MS combination), ion lenses, electrostatic mirrors[7] or guides,[8] position-sensitive detectors,[9–16] etc. Ion beam monitoring[10,11] and visualization of photofragment imaging[12,13] of jet-cooled molecules (i.e., spatially localized) have been performed using time-of-flight and two-dimensional detection capability.

In this article, a similar combination of time-of-flight and two-dimensional position-sensitive *XY* detection techniques is developed for analysis of ion dynamics in large volume gas cells. The goal is to investigate the potentialities of such a combination for mapping the acceleration fields of ions produced by the projectile-gas collisions. Other useful applications could be: digital recording of the projectile beam (including its spectroscopy), to help in the design of atomic collision spectrometers for initial momentum measurements and to extend mass spectrometry to large gas cells without losing mass resolution. This last feature comes from the fact that in ordinary TOF mass spectrometry, narrow peaks are obtained when ion sources very small (or distributed near a plane parallel to the detector) are employed; it is a good definition of the beam trajectory, combined to the *XY*-dectection capability, that allow the determination of the ion initial coordinates for a gas cell of any size. Exact and approximated expressions are presented for the functions $x_D(T)$ and $y_D(T)$, i.e., the impact position coordinates on the ion detector as a function of the ion time-of-flight T. The analytical properties of the $x_D(T)$ function are discussed. After describing the experimental setup, the method is applied for a spectrometer in which an inhomogeneous acceleration was intentionally provoked for sensitivity tests.

II. THEORETICAL BACKGROUND

A. Spectrometer structure

An overview of the *XY*-TOF spectrometer for projectile-gas collision analysis is depicted in Fig. 1. The (horizontal) *XZ* plane is defined by the beam trajectory and by the spectrometer symmetry axis; the (vertical) *Y* direction is perpendicular to this plane. Three electrodes define the electric field distribution inside the spectrometer: electrode 1 (at potential U_1) stops or is crossed by the beam, electrode 2 (at potential U_2) is constituted by a high transmission grid, and electrode 3 (grounded) is the entrance surface of the ion detector. The ions produced in the beam-gas collision are accelerated towards the grid by the electric field we want to determine and, after the grid, a uniform electric field assures adequate conditions for ion detection.

B. Definition of parameters

The necessary parameters for describing the gas ion dynamics parameters are defined in Fig. 2. The projectile incidence angle is θ_p. The gas molecule ionization occurs at the projectile coordinates $x_p, y_p=0$, $z_p=x_p$ cotg θ_p and at time $t_p=x_p/(v_p \sin \theta_p)$ before the projectile impact on electrode 1; v_p is the projectile velocity. The reference time T is set to zero when the projectile arrives at the coordinate origin. The

a)Author to whom correspondence should be addressed; electronic mail: enio@fis.puc-rio.br

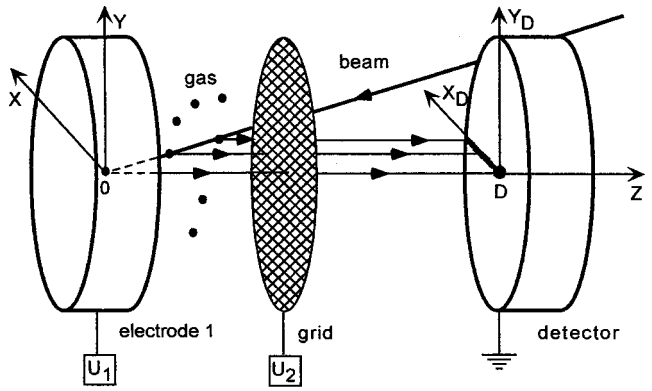

FIG. 1. *XY*-TOF spectrometer. The *Z* symmetry axis and the ionizing beam define the *XZ* plane and the *Y* direction. X_D and Y_D are the detector coordinate axes. A grid separates the first acceleration region (in which the determination of the electric field distribution is wanted) from the second one (where the field is uniform). Secondary ions, emitted by the spot O on the electrode 1 surface, are detected around detector center *D*. The ionized gas molecules are detected close to the X_D axis.

gas molecule ion is emitted with velocity v_0 in the direction given by the angle θ with the *z* axis, in a plane forming an angle φ with the *XZ* plane.

For time-of-flight measurements, the relevant parameters are the axial distances and the local axial component of the acceleration field. This acceleration is determined by the electric and/or magnetic force resultant. To illustrate analytically the method, a cylindrical configuration with three acceleration regions is considered, as shown in Fig. 2. Electrode 1, at potential U_1, is considered to be a conductor disk surrounded by a flat ring of inner radius *R* and thickness d_1'. The acceleration field in the first region is assumed to abruptly changed from ε_1 to ε_1' at the cylindrical surface defined by $x_p=R$.

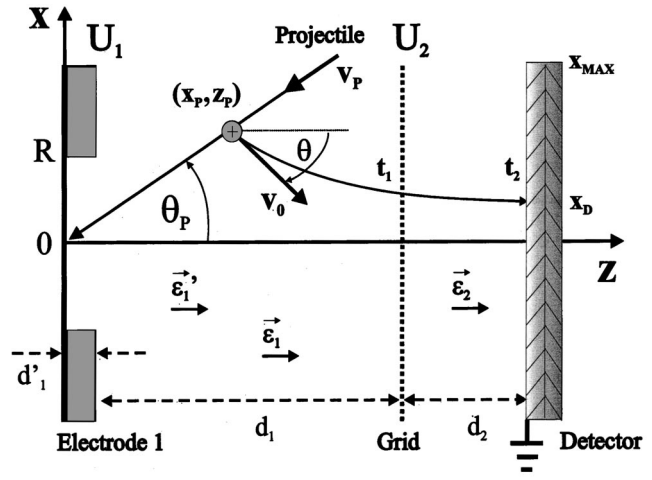

FIG. 2. *XZ*-plane view of the *three-acceleration-field spectrometer.* The projectile crosses the origin $x=y=z=0$ at the time $T=0$. The gas ion is produced at the point $(x_p, y_p=0, z_p)$ at the time t_p and is emitted with velocity $\mathbf{v}_0$ in the direction defined by θ and φ. The angle φ (not shown) is given by the *X* axis (horizontal) and the v_0 radial component. The first region has two subregions, defined by the cylindrical surface of radius *R* corresponding to the step in electrode 1. x_{max} is the detector radius and x_D is the *x* coordinate of the ion impact point on the detector surface. The electric field components ε_x and ε_y are kept at zero; ε_z is constant inside each subregion.

C. Position and TOF equations

After the total time-of-flight $T+t_p=t_1+t_2$, where t_1 and t_2 are, respectively, the times of flight in the first and second acceleration regions, the gas molecule ion reaches the (grounded) detector surface at the point coordinates:

$$x_D=x_p+v_0(T+t_p)\sin\theta\cos\varphi,$$
$$y_D=v_0(T+t_p)\sin\theta\sin\varphi, \tag{1}$$
$$z_D=d_1'+d_1+d_2.$$

The ion detection time is

$$T=t_1+t_2-t_p=\frac{d_1+d_1'-z_p}{(v_{0z}+v_{1z})/2}+\frac{d_2}{(v_{1z}+v_{2z})/2}$$
$$-\frac{z_p}{v_p\cos\theta_p}, \tag{2}$$

where v_{0z}, v_{1z}, and v_{2z} are, respectively, the axial velocities of the ionized gas molecule at the collision, grid crossing, and detector arrival instants, respectively:

$$v_{0z}=v_0\cos\theta, \tag{3}$$

$$v_{1z}=\sqrt{v_{0z}^2+\frac{2q}{m}(U_1-U_2)\left(1-\frac{z_p-d_1'}{d_1}\right)}\quad \text{if } x_p>R, \tag{4}$$

$$v_{1z}=\sqrt{v_{0z}^2+\frac{2q}{m}(U_1-U_2)\left(1-\frac{z_p}{d_1+d_1'}\right)}\quad \text{if } x_p<R, \tag{5}$$

$$v_{2z}=\sqrt{v_{1z}^2+\frac{2q}{m}U_2}. \tag{6}$$

These expressions hold for $R/d_1'>tg\ \theta_p>x_{max}/(d_1+d_1')$, a condition that guarantees that ionization should occur only in the first acceleration region.

D. Initial velocities

The initial velocity v_0 of the ionized gas molecule or atom is caused by three terms: (i) gas thermal motion; (ii) linear momentum conservation in the collision with the projectile, followed by electron emission or transfer; and (iii) for multiatomic target gases, Coulomb explosion process, or dissociation of unstable ion into neutral and ion fragments.

The first term can be determined from

$$\tfrac{1}{2}mv_{0z}^2=\tfrac{1}{2}kT_G,\quad \text{i.e.,}\quad v_{0z}^2=kT_G/m. \tag{7}$$

The momentum conservation in the projectile-gas collision also gives the contribution for v_0; however, this effect is usually negligible compared to the room-temperature (T_G) thermal motion.[17] On the contrary, Coulomb explosion contributions[18–20] are larger than the thermal ones and produce broad lines for $T(x_p)$ when integrated over all θ and φ emission angles. Unimolecular dissociations in which at least one fragment is a neutral release much less than the kinetic energy[4] (~order of eV) than in Coulomb explosion[18] (may be larger than 10 eV).

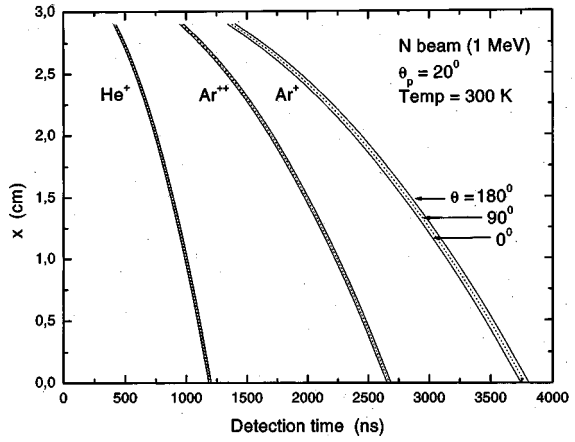

FIG. 3. x coordinate of the collision point as a function of the detection time. Each group of lines corresponds, respectively, to the indicated gas species and is calculated for three directions of ion emission with respect to the acceleration field, respectively. The group line broadening is due to thermal movement of the gas.

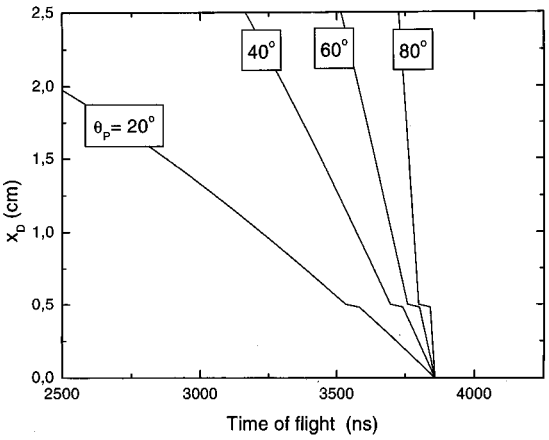

FIG. 4. $x(T)$ analytical calculations resulting of the beam scanning over the projectile angle.

An illustration of the $x_p(T)$ function, using Eqs. (2)–(6), is presented in Fig. 3 for the ion species: ($m_1=4$ u, $q_1=1$ e), ($m_2=40$ u, $q_2=1$ e), and ($m_3=40$ u, $q_3=2$ e); the gas temperature is $T_G=300$ K and the spectrometer configuration is $d_1=9.0$ cm, $d_1'=0$, $d_2=1.0$ cm; $U_1=3.0$ kV, and $U_2=2.5$ kV. As expected, the predicted times of flight increase as $\sqrt{m/q}$. It should be pointed out that the slope dx_p/dT is not always negative: if the ratio d_2/d_1 is large enough, this derivative becomes positive for large or for all x_p values. The effect of the thermal velocity v_0 on $T(x_p)$ causes the line broadening, which also increases as $\sqrt{m/q}$.

Introducing Eq. (7) into Eqs. (2)–(6), an interesting property appears for $T(x_p)$: the quantity $\sqrt{m}$ can be factorized from t_1 and t_2, so that the *reduced time-of-flight*

$$T_{\mathrm{red}}(x_p) \equiv \left(T + \frac{x_p}{v_p \sin \theta_p} \right) \frac{1}{\sqrt{m}}, \tag{8}$$

becomes a universal function for all ionized species with the same charge state. Actually, this property holds even for accelerating regions with inhomogeneous electric fields and may be used as field mapping. The $T_{\mathrm{red}}(x_p)$ function can be seen as the time of flight for a gas ion having $m=1$ mass and produced by a $v_p \to \infty$ projectile. The $T_{\mathrm{red}}(x_p)$ function may be plotted with exchanged axes, i.e., inverted into the $x_p(T_{\mathrm{red}})$ function, for easier comparison with experimental data.

E. Field mapping

As the ion TOF depends on the acceleration field distribution along the region delimited by the projectile trajectory and the XY detector, it can be used for mapping this distribution. The general problem of getting the field from the (x_D, y_D, and T) set of measurements is complex or may lead to an ambiguous solution. Some solving procedures may be attempted, such as: (i) to assume a function for the field distribution and determine the values of its parameters from data fittings; (ii) to assume an initial field distribution and calculate deviations, and (iii) to get additional experimental data by varying the position of the ionization sites, which can be achieved by rotating the gas cell or scanning it with the ionizing beam. The simplest situations are those for which only time-independent electrostatic fields exist.

For the illustration considered in this work [Eqs. (1)–(6)], the field homogeneity is broken by a thin circular well created in electrode 1, with radius $R=0.5$ cm and height $d_1'=0.2$ cm. The effect of beam scanning on $x_p(T)$ is analyzed by using Eq. (4) or (5) for different projectile directions θ_p. Results of the simulation, presented in Fig. 4, show that the relative small indent in electrode 1 produces a visible change in the gas ion time of flight for all incidence angles.

The simulation using Eqs. (4) and (5) is practical because the corresponding field distribution is close to reality and T is determined analytically. Close to $x=R$ an incorrect feature may be anticipated, once the field given by the model changes abruptly and has no radial component. As a consequence, the function $x(T)$ must present a discontinuity at this border and its slope should not vary much. A more realistic field distribution is found in this case by solving the Laplace equation numerically, e.g., through the SIMION code.[21] In Fig. 5, the results from SIMION (dotted line) are compared with Eqs. (4) and (5) analytical model predictions (solid

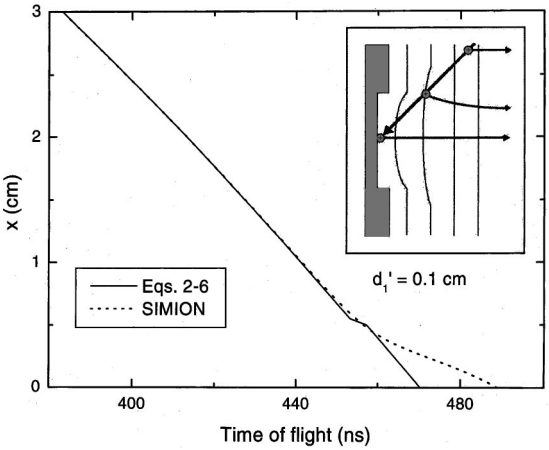

FIG. 5. $x(T)$ functions given by the analytical model [Eqs. (2)–(6)] and by the Simion code. Note the agreement for large x and the different slopes for low x caused by different field distortions considered in the two models.

line). For $x \gg R$, the field is homogeneous and the two models give identical predictions. Visible differences between them occurs for $x < R$, due to the existence of: (i) a negative radial component of the electric field which approaches the gas ion towards the spectrometer axis, increasing its trajectory length and (ii) a smaller axial component which increases its time of flight, changing the $x(T)$ slope. If $d_1' \ll R$ the $x(T)$ slope close to $x=0$ becomes again the same for the two approaches, once the electric field homogeneity at the spectrometer axis is not disturbed by the electrode step at $x=R$.

F. Approximated equations

In order to examine analytically the average ion impact position on the detector ($\overline{x_D}$) as a function of T, it is convenient to approximate Eq. (2) for small initial velocities ($v_0 \ll \underline{v_{1z}}$) and for collisions close to the spectrometer axis ($x_p \approx x_D \ll x_{\max}$); d_1' is set equal to zero for simplicity. Under these conditions, Eq. (5) may be approximated by

$$v_{1z} \approx \sqrt{\frac{2q}{m}(U_1 - U_2)}\left(1 - \frac{1}{2}\frac{x_p}{d_1\ tg\,\theta_p}\right). \tag{9}$$

Therefore,

$$T \approx \sqrt{\frac{2m}{q}}\left[\frac{d_1}{\sqrt{U_1-U_2}} + \frac{d_2}{\sqrt{U_1-U_2}+\sqrt{U_2}} + \frac{a}{2tg\ \theta_p}x_p\right] - \frac{x_p}{v_p \sin\theta_p}, \tag{10}$$

where

$$a = \frac{d_2}{d_1}\frac{\sqrt{1-U_2/U_1}}{\sqrt{U_1-U_2}+\sqrt{U_2}} - \frac{1}{\sqrt{U_1-U_2}}. \tag{10a}$$

From Eq. (10), one gets the slope of the $T(x_p)$ function:

$$\frac{dT}{dx_p} = \sqrt{\frac{m}{2q}}\frac{a}{tg\ \theta_p} - \frac{1}{v_p \sin\theta_p}. \tag{11}$$

The following properties can be predicted:

(i) The $v_0 \approx 0$ approximation obviously implies in the same universal function, $T_{\mathrm{red}}(x_p)$, given by Eq. (8).

(ii) The time of flight becomes independent of x_p, in first-order approximation, if $dT/dx_p = 0$. This situation occurs when

$$a = \frac{\sqrt{2q/m}}{v_p \cos\theta_p}. \tag{12}$$

(iii) For very fast projectiles, dx_p/dT is proportional to $tg\ \theta_p/\sqrt{m}$ and diverges when $a \approx 0$, i.e., when

$$\frac{d_2}{d_1} = \frac{1+\sqrt{(U_2/U_1)/(1-U_2/U_1)}}{\sqrt{1-U_2/U_1}}, \tag{13}$$

which corresponds to the Wiley and McLaren[3] condition for time focusing in the Z direction.

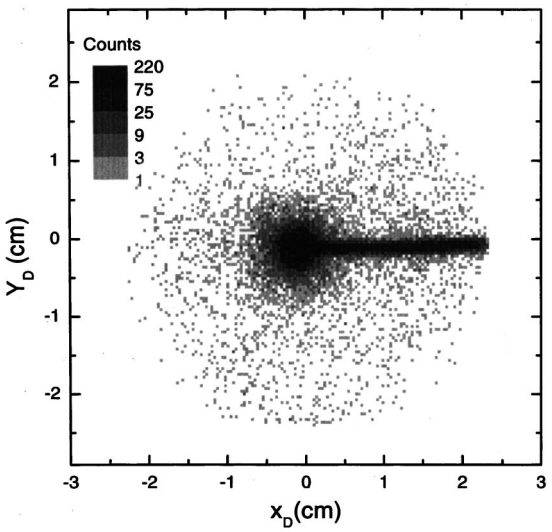

FIG. 6. *XY* spectrum of the ion impact on detector. The line on the *X* direction corresponds to the projection of the beam trajectory on the detector (see also the axes *X* and *Y* in Fig. 1). The beam goes from the right to the left and impacts electrode 1 at coordinates $x=y=0$, producing secondary ions which create the central peak.

(iv) If $U_2 = 0$ (i.e., one single acceleration region), Eq. (12) becomes $a = [(d_2/d_1)-1]/\sqrt{U_1}$; then $dx_p/dT \sim \sqrt{U_1}$, and diverges when $d_2 = d_1$.

(v) For grazing incidence ($\theta_p \sim 90°$), $tg\ \theta_p$ becomes very large and $dx_p/dT \approx v_p$.

III. EXPERIMENTAL RESULTS

The characteristics of the *XY*-TOF spectrometer have been described elsewhere.[15,16] A continuous flow of a 70% He, 15% Ne, and 15% Ar gas mixture was introduced in the spectrometer, in such a way that the gas pressure inside the cell was kept at 10^{-5} mbar. The gas was bombarded with a 150 keV neutral hydrogen beam produced by the Van de Graaff accelerator of the Institute für Kernphysik of the J. W. Goethe University. Start signals for the TOF system were given by a secondary electron detector placed behind a thin foil (electrode 1 in Fig. 2).

The spectrometer parameters for these measurements were: $U_1 = 2.970$ kV; $U_2 = 0.040$ kV; $d_1 = 8.41$ cm; $d_1' = 0.01$ cm; $d_2 = 0.7$ cm, and $\theta_p = 37°$ or $77°$. The beam diameter was about 10^{-2} cm. Gas temperature T_G was considered to be 300 K, and therefore, the average atomic kinetic energy is $E_0 \sim 39$ meV. Figure 6 presents the *XY* graph of the data, integrated over all times of flight; one sees a line in the x direction that represents the projection of the beam trajectory inside the spectrometer. The line thickness is mainly attributed to the thermal motion of the gas molecules, each point corresponding to the detection of an ion produced by the beam–gas collision. The beam diameter also contributes to the line thickness.

Figure 7(a) presents an *XY* graph of the ions produced by the beam collision. Oblique lines relative to the $x(T)$ function for each gas species can be seen, as well as vertical lines crossing the T axis due to secondary ions desorbed from electrode 1. The projection of the same data over the T axis generates the usual time-of-flight spectrum, as shown in Fig. 7(b).

Figure 8 presents $x(T)$ experimental data (black circles) for a He gas target bombarded by H at the projectile angle

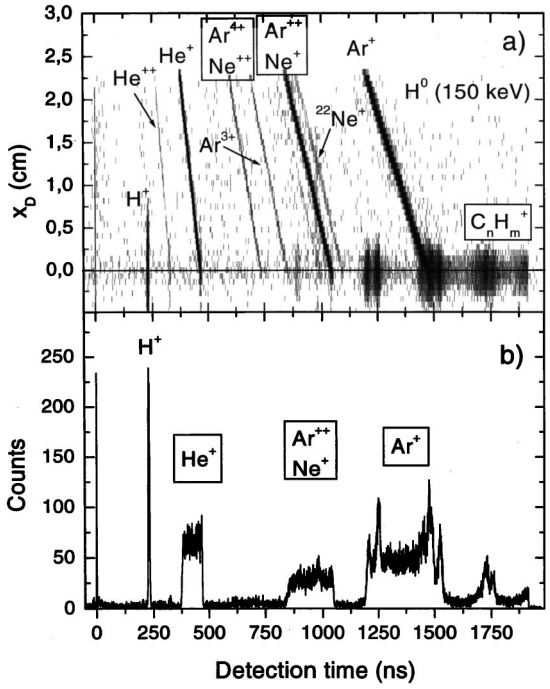

FIG. 7. (a) Experimental $x(T)$ spectrum of He, Ne, and Ar gases bombarded by a 150 keV H^0 beam. Incidence angle is $\theta_p = 37°$. The points close to the T axis ($x=0$ line) and forming vertical lines are due to secondary ions emitted by electrode 1. Events from the beam–gas collision generate oblique lines for $x>0$. (b) TOF spectrum, i.e., projection of the $x(T)$ data on the T axis. The thin peaks are due to the ions desorbed from the electrode, while the gas ions generate the broad peaks.

$\theta_p = 77°$. One sees the effect of collisions in the two different subregions: close to the T axis, the extraction field is $d_1'/d_1 \approx 1\%$ smaller than in the outer subregion. This difference is, however, enough to cause a visible TOF increase for He^+ ions. The solid line is the prediction of the Eqs. (2)–(6) model, as discussed in the next section.

IV. DISCUSSION AND CONCLUSIONS

The present method is based on three considerations:

(1) For an electric field distribution that is not too complex, the reconstruction of the gas ion trajectory is possible from the knowledge of the ion time-of-flight T, from the $z_p = z_p(x_p, y_p)$ beam trajectory, and from the final positions of the ion, i.e., the (x_D, y_D) impact coordinates on the detector. In other words, starting from the beam trajectory equation and from the measured (x_D, y_D, T) set, it is possible to determine the ion coordinates x_p, y_p, and z_p as well as its initial velocity v_0.
(2) The accuracy in time (subnanosecond) and in XY position (submillimeter) measurements of the detector/acquisition system provides a very sensitive tool for the ion dynamics after the collision.
(3) Eventual ambiguities in the acceleration field distribution may be solved by varying the beam trajectory.

An efficient procedure to test the model described in Sec. II is to construct the reduced time of flight for the experimental data. The results, presented in the $x(T_{red})$ format, are shown in Fig. 9 for the He, Ne, and Ar data. A very good

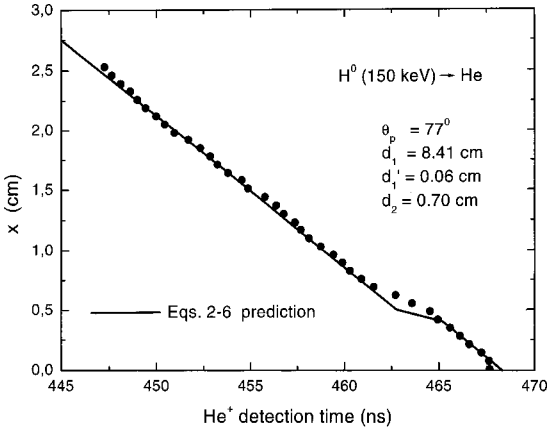

FIG. 8. Dots are the $x(T)$ spectrum for grazing projectile incidence on electrode 1, a situation in which the $x(T)$ slope is high. Note the sensitivity to field nonhomogeneities around $x = R = 0.5$ cm. The solid line is Eqs. (2)–(6) prediction, in very good agreement with data.

overlap of the corresponding points is obtained for $T_{red}(x_p)$. Small discrepancies occur for very low or very large x values: they are attributed to field nonhomogeneities near, respectively, the electrode 1 flat ring and of the XY-detector border. The presentation of all data by a single universal curve demonstrates that, indeed, the different flying ion species are submitted to the same electrostatic field distribution. The two solid lines in Fig. 9 represent the Eq. (2) predictions, using the spectrometer parameters of Sec. III; one line corresponds to $\theta = 0$ (ion emission towards the detector) and the other one to $\theta = 180°$.

In conclusion, the method of combining the time-of-flight technique with position-sensitive detection opens interesting new possibilities of observing the track of an ionizing projectile (photon or particle) in gas chambers. In particular, the use of pulsed lasers provides a practical method for scanning the chamber interior in the regions of interest for field mapping.

Concerning mass spectrometry, the comparison between Figs. 7(a) and 7(b) shows why it is still possible to analyze large volume gas targets with good mass resolution far away

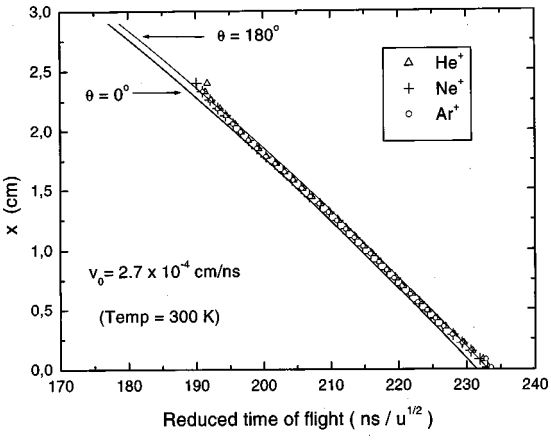

FIG. 9. Experimental and calculated $x(T_{red})$ graph, i.e., the x collision coordinate plotted vs the reduced time of flight. It is of interest to emphasize that in such a graph the $x(T)$ data for all ion species are reduced into a single, universal curve.

from the Wiley–McLaren time focusing conditions.[16] This volume depends essentially on: the detector area ($\pi\phi^2/2$), the electrode-grid distance (d_1), and the projectile incidence angle (θ_p). The parameters used in the current setup are ϕ=5.0 cm, d_1=8.4 cm, and $\theta_p^{\min}=\phi/2d_1=16°$.

The *XY* detection capabilities allow the initial momentum analysis of the ions generated in the projectile-gas collisions. The sensitivity of the method to initial velocities can be estimated from the $x(T)$ line thickness given either by the model (Figs. 3 and 9) or by the presented data [Figs. 5 and 6(a)].

ACKNOWLEDGMENTS

The DAAD/CAPES-PROBAL program is gratefully acknowledged for making possible the collaboration between IKF and PUC-Rio. PADCT and FAPERJ are also acknowledged for their partial support of the investigations. The authors thank Dr. V. M. Collado for his help in writing the software for the theoretical calculations and L. F. Amorim for running the SIMION code.

[1] R. J. Cotter, *Time-of-Flight Mass Spectrometry* (ACS Professional Reference Books, Washington, DC, 1997); see, in particular the chapter ''Overview and History.''
[2] B. A. Mamyrin, Int. J. Mass Spectrom. Ion Processes **206**, 251 (2001).
[3] W. C. Wiley and I. H. McLaren, Rev. Sci. Instrum. **26**, 1150 (1955).
[4] J. H. Beynon, *Mass Spectrometry and Its Applications to Organic Chemistry* (Elsevier, Amsterdam, 1960).
[5] E. W. Schlag, Int. J. Mass Spectrom. Ion Processes **131**, R9 (1994).
[6] M. L. Vestal, P. Juhasz, and S. A. Martin, Rapid Commun. Mass Spectrom. **9**, 1044 (1995).
[7] B.A. Mamyrin, V. I. Karataev, D. V. Shmikk, and V. A. Zagulin, JETP **37**, 45 (1973).
[8] K. V. Davis, E. F. da Silveira, and E. A. Schweikert, Nucl. Instrum. Methods Phys. Res. A **273**, 203 (1988).
[9] O. Becker and K. Wien, Nucl. Instrum. Methods Phys. Res. B **16**, 456 (1986).
[10] M. Unverzagt, H. E. Berg, J. Ulrich, B. Franzke, W. Bourgeois, R. Mann, and H. Schmidt-Böcking, GSI Annual Report (1991), p. 437.
[11] M. Unverzagt, J. Ulrich, B. Franzke, W. Bourgeois, and H. Schmidt-Böcking, GSI Annual Report (1992), p. 449.
[12] A. J. R. Heck, Eur. Mass Spectrom. **3**, 171 (1997).
[13] L. McDonnell and A. J. R. Heck, J. Mass Spectrom. **33**, 415 (1998).
[14] M. Most, K. Wien, A. Brunelle, S. Della Negra, J. Depauw, D. Jacquet, M. Pautrat, and Y. LeBeyec, Nucl. Instrum. Methods Phys. Res. B **168**, 203 (2000).
[15] T. Jalowy, R. Neugebauer, M. Hattass, J. Fiol, F. Afaneh, J. A. M. Pereira, E. F. da Silveira, H. Schmidt-Böcking, and K. O. Groeneveld, Nucl. Instrum. **193**, 762 (2002).
[16] T. Jalowy, R. Neugebauer, K. O. Groeneveld, C. R. Ponciano, L. S. Farenzena, and E. F. da Silveira, Int. J. Mass Spectrom. (to be published 2002).
[17] M. A. Abdallah, C. R. Vane, C. C. Havener, D. R. Scultz, H. F. Krause, N. Jones, and S. Datz, Phys. Rev. Lett. **85**, 278 (2000).
[18] D. S. Gemmell, Nucl. Instrum. Methods Phys. Res. **191**, 425 (1981).
[19] E. P. Kanter, P. J. Cooney, D. S. Gemell, K. O. Groeneveld, W. J. Pietsch, A. J. Ratkowski, Z. Vager, and B. J. Zabransky, Phys. Rev. A **20**, 834 (1979).
[20] D. S. Gemmell, Phys. Today **37**, S25 (1984).
[21] Simion 3D code, version 6.0, D. A. Dahl, Idaho National Engineering Laboratory (1995).